Journal of Materials Chemistry A

RSC Publishing

PAPER

View Article Online
View Journal | View Issue

Cite this: J. Mater. Chem. A, 2013, 1, 1246

Formation of WO_3 nanotube-based bundles directed by $NaHSO_4$ and its application in water treatment†

Jin Li, Xiaoheng Liu,* Qiaofeng Han, Xiaxi Yao and Xin Wang*

Self-assembly can offer a very powerful tool for the design of novel materials and many different templates have been found to direct the formation of microstructures. In this article, we report a simple method for the self-assembly of three-dimensional (3D) WO_3 nanotube bundles. It is demonstrated that not only can $NaHSO_4$ act as a reactant, but also, more importantly, it played multiple key roles in the self-assembly processes, while NH_4HSO_4 and $KHSO_4$ have none of these functions at all. As suggested, at first, WO_3 ordered and layered structures can be generated by the hydrothermal reaction of $NaHSO_4$ with Na_2WO_4 at 180 °C, and then sodium ions (Na^+) inserted into the layer cause a continual curl of the WO_3 outer-slice by the repel force of static electricity between Na^+ ions and H^+ ions on the surface of the WO_3 slice. Herein, Na^+ ions can dramatically promote the formation of WO_3 single crystal slices, which are precursors of the self-assembly, and SO_4^{2-} ions can bridge the WO_3 slices as well as the nanotubes. In addition, it is found that the WO_3 nanotube bundles still keep their original aggregation after template removal, and the bundle can be disassembled gradually under a long treatment time of aqueous ultrasonication. Furthermore, the application in wastewater treatment of WO_3 nanotube bundles has been investigated.

Received 20th September 2012
Accepted 7th November 2012

DOI: 10.1039/c2ta00382a

www.rsc.org/MaterialsA

1 Introduction

It is well-known that self-assembly is a fundamental phenomenon that generates structural organization on micron- and nano-sized scales, and the self-assembly of nanocrystals of specific morphology has aroused great attention due to their interesting properties and many applications.[1] Accordingly, the development of rational approaches to assemble nanoscale building blocks into definite structures is still desirable and significant, which would greatly promote their applications in nanodevices. In particular, two- or three-dimensional hierarchical nanostructures with tailored morphologies and patterns built from nanowires, nanorods, nanotubes, or other nanocrystals have drawn intensive research interest.[2] Over the past decade, besides the spontaneous self-assembly of nanocrystals into hierarchical nanostructures by oriented attachment,[3] self-assembly methods with templating assistance, such as Langmuir–Blodgett films, organic surfactants and copolymers, and DNA have also been commonly used to direct assembly to construct the complicated structures.[4] Tubular nanostructures have been widely utilized in various areas due to their unique shape, such as catalysis, fluidics, purification, separation, gas storage, energy conversion, sensing, drug release, and so on.[5] Though many researchers have focused on single nanotubes, nanotube bundles also attract people's attention. Up to now, significant progress has been made recently on the synthesis of nanotubes of different materials,[6] but very few works have focused on understanding and mastering their assembly. Especially, the self-assembly of nanotube bundles is still poorly understood. So it still remains a challenge to develop a facile method to organize nanotubes with ordered arrays and good shape homogeneity for current research.

As an important n-type semiconductor, tungsten trioxide has received considerable attention owing to some outstanding properties. It is used for instance in electronic devices, catalysts, gas sensors, splitting water and rechargeable lithium-ion batteries, as well as in other fields.[7] Many efforts have been devoted to the fabrication of nanostructured tungsten trioxide to enhance and improve its performance in the above applications. The synthesis of tungsten trioxide nanostructures has been reported through a variety of reaction protocols, including the template method, electrochemical techniques, combustion synthesis, chemical vapor deposition, hydrothermal reaction, sol–gel approach, and flame spray pyrolysis process.[8] To date, using the above methods, various high-quality WO_3 nanostructures, such as nanofibers, nanorods, nanotrees, nanotubes and nanoplates, have been fabricated.[9] Recently, numerous efforts have been focused on the growth and assembly of crystalline tungsten oxide nanostructures.[10] However, little success has yet been achieved in the controlled synthesis of WO_3 nanotubes and nanotube bundles until recently.

Key Laboratory of Education Ministry for Soft Chemistry and Functional Materials, Nanjing University of Science and Technology, Nanjing 210094, China. E-mail: wangx@mail.njust.edu.cn; xhliu@mail.njust.edu.cn

† Electronic supplementary information (ESI) available. See DOI: 10.1039/c2ta00382a

Here, we demonstrate the synthesis of WO_3 nanotube bundles, including its disassembled products *via* a simple hydrothermal method, without using any traditional templates, surfactants, or various substrates. The WO_3 nanotube bundle superstructures, based on one-dimensional (1D) nanoscale building blocks, have been prepared. To the best of our knowledge, this is the first report on a controllable hydrothermal synthetic method for the selective growth and assembly of tungsten trioxide nanotubes into well-defined three-dimensional (3D) nanostructures. A possible formation mechanism for the bundle-like structure was proposed as well. In addition, as an example of a potential application, the tungsten trioxide obtained was tested as an adsorbent for wastewater treatment.

2 Experimental section

2.1 Materials

$NaHSO_4 \cdot H_2O$, NH_4HSO_4, $KHSO_4$ and $Na_2WO_4 \cdot 2H_2O$ employed in this research are commercially available products. All reagents were used without further purification.

2.2 Synthesis of WO_3 nanotube bundles

In a typical experimental, 0.99 g of $Na_2WO_4 \cdot 2H_2O$ and 1.19 g of $NaHSO_4 \cdot H_2O$ were dissolved in 40 mL of deionized water to form the precursor solution, which was then transferred into a Teflon-lined stainless steel autoclave with a capacity of 50 mL. The autoclave was sealed and hydrothermally treated at 180 °C for 24–48 h. After the autoclave cooled down to room temperature naturally, the resulting precipitates were collected by centrifugation and washed several times by deionized water and ethanol to remove possible impurities, and subsequently dried in air at 60 °C for 12 h.

2.3 Water treatment experiments

In this experiment, methylene blue (MB) was used as an organic pollutant. MB (20 mg L^{-1}, 10 mL) was mixed with the adsorbent (10 mg), and the adsorption process was monitored by a UV-vis spectrophotometer (Shimadzu UV-2550) at given time intervals. The adsorption isotherm was obtained by different MB concentrations with stirring for 12 h at room temperature.

2.4 Characterization

The X-ray powder diffraction (XRD) patterns were recorded on a Bruker D8 Advance diffractometer with Cu Kα radiation (λ = 1.5406 Å) at 45 kV, 40 mA. The diffraction data were recorded for 2θ angles between 10° and 70°, and the small angle X-ray diffraction (SAXD) data were recorded for 2θ angles between 0.5° and 5°. Morphologies of the as-obtained products were observed using field emission scanning electron microscopy (FESEM, Quanta 400 FEG, FEI) and scanning electron microscopy (SEM, JEOL-6380LV). Structural and compositional investigations using transmission electron microscopy (TEM and HRTEM) and X-ray energy dispersive spectroscopy (EDS) were performed on a JEOL-2100 with an accelerating voltage of 200 kV. X-ray photoelectron spectra (XPS) were recorded on a Perkin-Elmer PHI5300 X-ray photoelectron spectrometer, using Al Kα ($h\nu$ = 1486.7 eV) X-ray as the excitation source. Moreover, the Brunauer–Emmett–Teller (BET) surface area and pore volume were measured by the nitrogen gas adsorption–desorption method at 77 K using a TriStar II 3020 Micrometrics apparatus. The pore size distribution was calculated by the Barrett–Joyner–Halenda (BJH) method using the desorption branch of the isotherm. Fourier-transform infrared (FTIR) spectroscopy (BRUKER, VECTOR 22) and Raman spectroscopy (Jobin Yvon, T64000 spectrometer with a 514.5 nm argon ion laser) were utilized to characterize the products.

3 Results and discussion

The morphologies of the as-synthesized products were examined by field-emission scanning electron microscopy. A representative field-emission scanning electron microscope image of the WO_3 products is shown in Fig. 1a at a low magnification for an overview, from which it can be seen that the as-obtained WO_3 nanostructures are mainly nanocolumns. In addition, Fig. 1b clearly exhibits that the nanocolumns are constructed from the assembly of smaller nanowires with a regular arrangement, and the diameter of the nanocolumn is approximately 70–120 nm. To gain more detailed information about the nanostructure of these WO_3 nanocolumns, XRD, TEM, HRTEM, and selected area electron diffraction analyses were performed, respectively. As shown in Fig. 2a and b, each nanocolumn is actually composed of a large quantity of well-defined nanotubes that are 10–20 nm in diameter and micrometer-sized in length. The WO_3 nanotube bundles can be disassembled under a long treatment time of aqueous ultrasonication, as illustrated in Fig. 2c. Nanotubes with diameters of about 12 nm and lengths of up to hundreds of nanometers were obtained. This phenomenon has presented more evidence of WO_3 nanotube formation and will be discussed at length.

Moreover, the phase purity and crystal structure of the WO_3 nanotube bundles have been confirmed by XRD. As shown in Fig. 3a, all the diffraction peaks can be exclusively indexed to a hexagonal tungsten trioxide crystalline phase (h-WO_3), with lattice constants of a = 7.298 Å and c = 3.899 Å (JCPDS # 33–1387), and no other impurities are observed from the XRD pattern. The strong and sharp diffraction peaks indicate good crystallinity of the as-synthesized products. A strongly preferential growth direction along the *c*-axis [001] can be found. A HRTEM image and a SAED pattern taken from a single nanotube are shown in Fig. 3b. Clear lattice fringes corresponding to the (200) crystalline plane of hexagonal WO_3 with *d*-spacing of 0.316 nm can be seen, indicating the single-crystal quality of a WO_3 nanotube. Combined with the SAED pattern (inset Fig. 3b) recorded on an individual nanotube, it is revealed that the as-prepared WO_3 product consists of single-crystalline nanotubes with a preferred orientation along the [001] direction, which is in accordance with the XRD result. Furthermore, the wall of a single WO_3 nanotube can also be seen clearly, and its thickness is estimated to be about 3 nm.

The surface composition and state of the product were further investigated using X-ray photoelectron spectroscopy

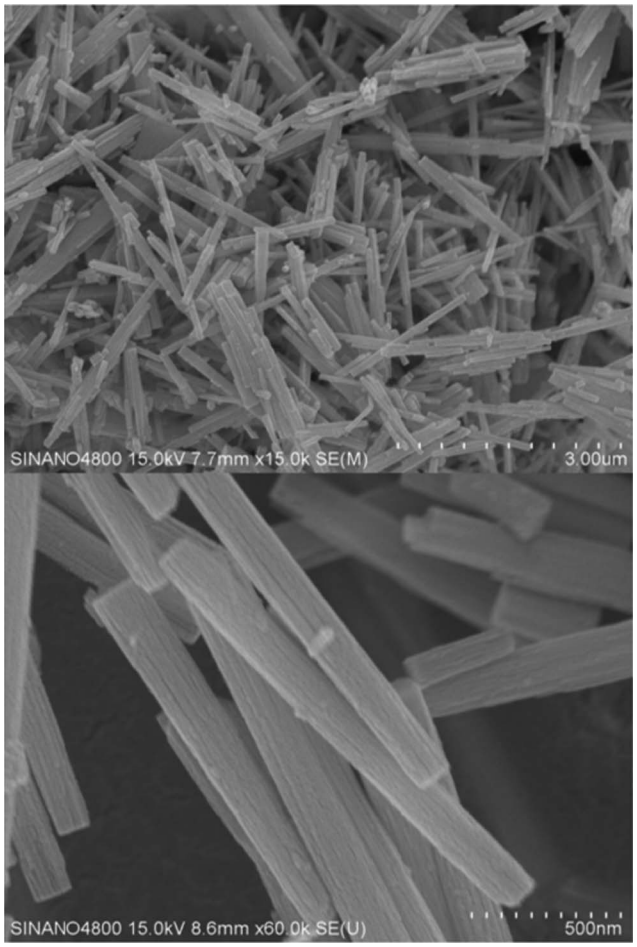

Fig. 1 FESEM images: (a) WO_3 products, (b) magnification of central area of (a).

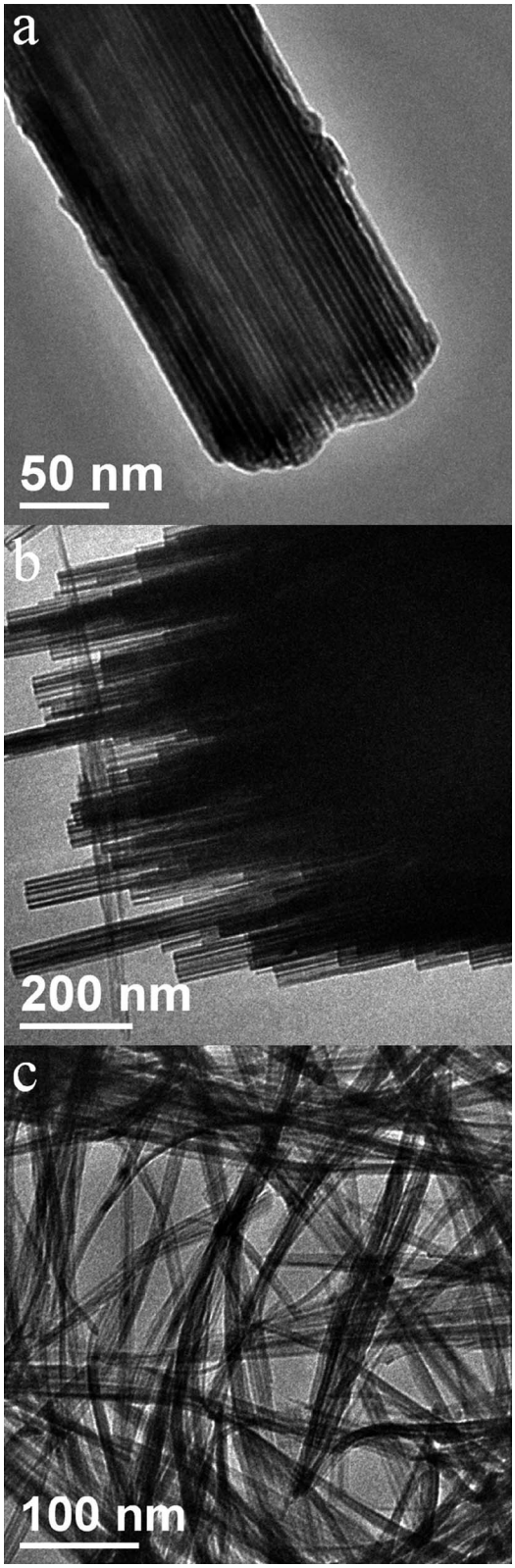

Fig. 2 TEM images of a WO_3 nanotube bundle: (a) and (b) with diameters of about 120 nm and 70 nm, (c) disassembly result.

(XPS). As shown in the wide-scan XPS spectrum (Fig. 4a), no obvious impurity peak can be detected. The XPS peak for C 1s at 285 eV is due to the adventitious hydrocarbon from the XPS instrument itself. The W 4f core-level value at 35.8 eV is very close to the reported value of 36 eV.[11] The W 4f spectrum (Fig. 4b) presents the 7/2–5/2 spin–orbit doublet for the W valence state, whereas the intense doublet at EB(W $4f_{7/2}$) = 35.5 eV and EB(W $4f_{5/2}$) = 37.7 eV corresponds to the W^{6+} oxidation state from WO_3. This result is consistent with the XRD analysis.

Raman spectroscopy was also used to characterize the structure of the as-synthesized nanotube WO_3 bundles, since this sensitive technique is suitable to obtain details of the WO_3 chemical structure (Fig. 4c). Well-defined Raman peaks centered at 110 cm^{-1}, 241 cm^{-1}, 326 cm^{-1}, 672 cm^{-1}, 755 cm^{-1}, and 810 cm^{-1} can be observed. According to the literature,[12–14] these bands can be assigned to the fundamental modes of crystalline h-WO_3. The bands at 755 cm^{-1} and 810 cm^{-1} in Fig. 4 are related to O–W–O stretching modes, while the bands at 241 cm^{-1} and 326 cm^{-1} can be attributed to the W–O–W bending mode of the bridging oxygen. The bands at 110 cm^{-1} below the 200 cm^{-1} modes are attributed to the lattice vibrations. A weak shoulder at 672 cm^{-1} is observed; it is a typical Raman peak of crystalline WO_3, which corresponds to the stretching and bending vibrations of the bridging tungsten and oxygen atoms.[15]

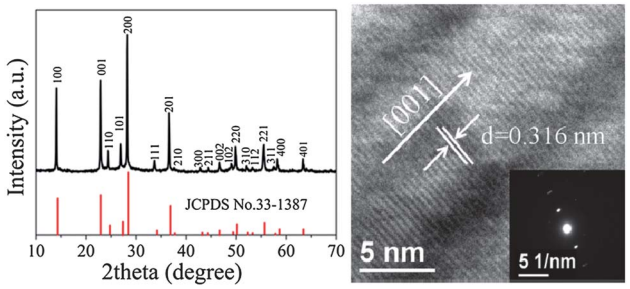

Fig. 3 (a) XRD pattern of WO_3 nanotube bundles and JCPDS no.33-1387, (b) HRTEM and SAED images of the WO_3 nanotube wall.

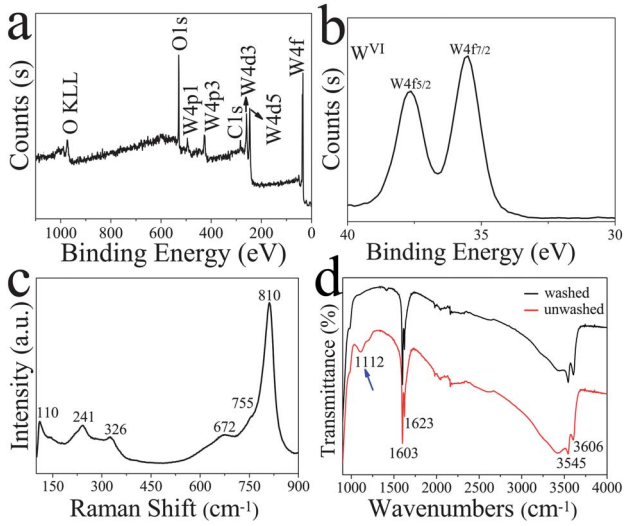

Fig. 4 Spectrum of the WO_3 nanotube bundle: (a) survey XPS spectrum and (b) W 4f core level region, (c) Raman spectra of the samples and (d) FTIR spectra of the samples: washed and unwashed.

In order to identify blocking from Na_2SO_4 inside the tube, FTIR was applied to analyse the residual amount of SO_4^{2-} ions. The above-mentioned XRD and XPS results clearly showed that the SO_4^{2-} ion is absent, because the absorbed sulfate ions were washed away from the products after washing. For the unwashed sample, it is found that the

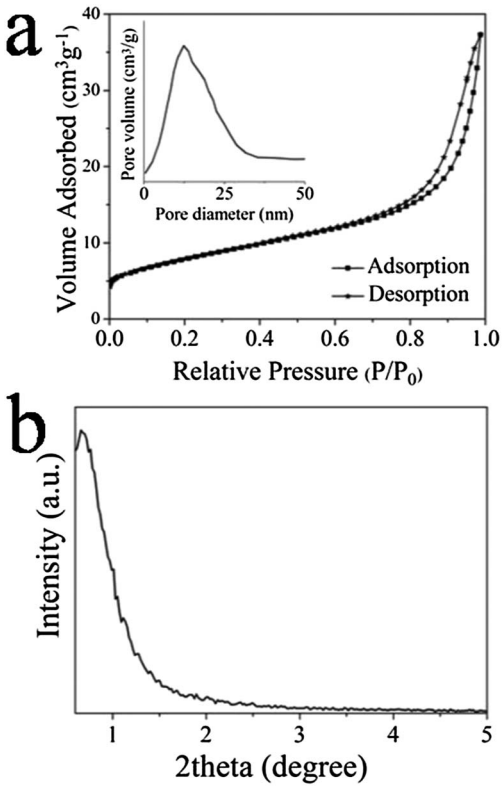

Fig. 5 (a) Nitrogen adsorption–desorption isotherm and the BJH pore size distribution curve of the products. (b) Small angle X-ray diffraction pattern.

asymmetric stretching mode of SO_4^{2-} appears as a very intense broad band at 1112 cm^{-1} in the FTIR spectrum (Fig. 4d).[16] Further evidence exhibits that the SO_4^{2-} ions are adsorbed on a specific surface of the nanotubes, and bridge between the nanotubes. In addition, the bending mode of adsorbed water is located at 1623 and 1603 cm^{-1}, and the region between 3800 and 3000 cm^{-1} contains bands due to both surface WOH and adsorbed water.[17] The surface –OH favors the formation of nanotubes, because it can adsorb more H^+ ions, which enhances the Na^+ repel force of static electricity among slices (see Scheme 1), and further speeding up the transformation from slices to nanotubes.

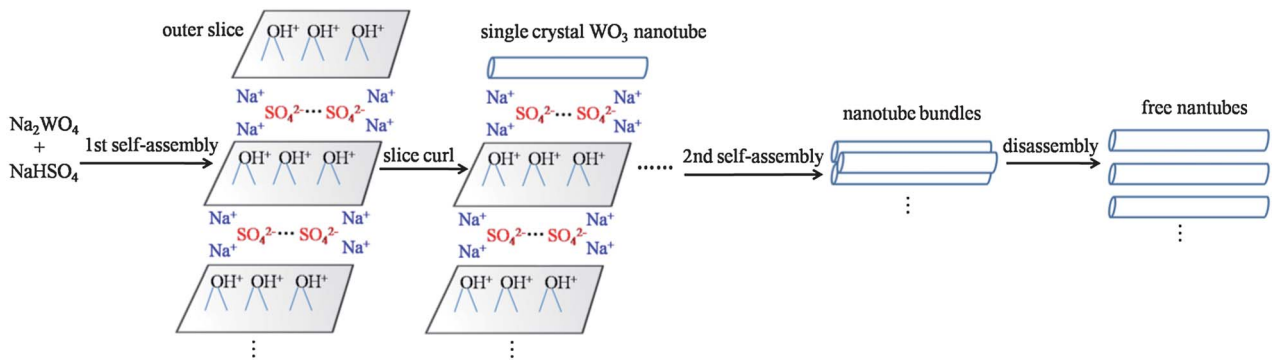

Scheme 1 Formation mechanism of ordered WO_3 nanotube bundle through two self-assembly steps.

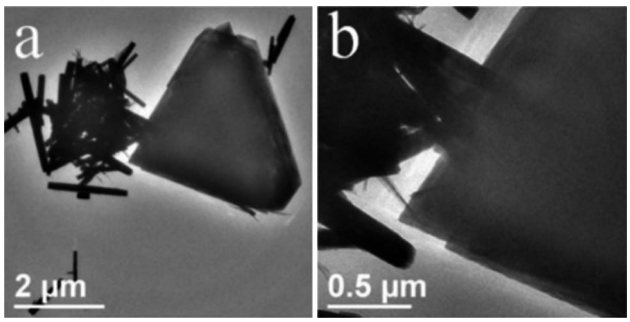

Fig. 6 TEM images: (a) both nanotube bundles and layered slices, (b) magnification of (a).

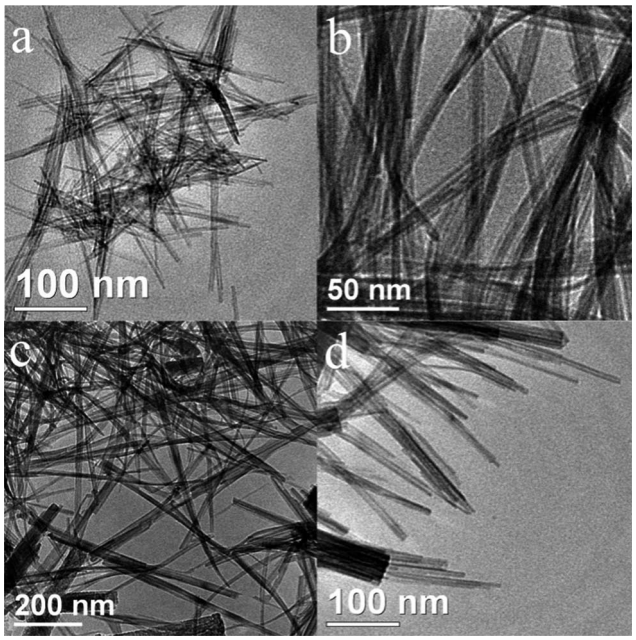

Fig. 7 TEM images: (a) and (b) disassembled WO_3 nanotubes, (c) and (d) mixed product of both WO_3 nanotubes and bundles.

Nitrogen adsorption–desorption isotherms were measured to determine the specific surface area and pore volume of the WO_3 nanotubes, and the corresponding results are presented in Fig. 5a. The isotherm displays a typical type IV curve with a hysteresis loop at relative pressure (P/P_0) between 0.4 and 1.0, suggesting the presence of mesopores in the products without a doubt.[18] Meanwhile, the small angle X-ray diffraction (SAXD) was utilized to further explain the existence of the orderly mesopores, and the result is shown in Fig. 5b. The pore diameter calculated from the SAXD data is about 13.2 nm, and such a small size is attributed to the mesopores. The two kinds of results are in agreement with each other. The plot of the pore size distribution (inset in Fig. 5a) is calculated by using the Barrett–Joyner–Halenda (BJH) method from the desorption branch of the isotherm. The BET data are also interesting and even puzzling, and are discussed in Table S1 and Scheme S1.† According to the BET method, a typical value for the specific surface area is about 27.83 $m^2\ g^{-1}$, a result which is confusing.

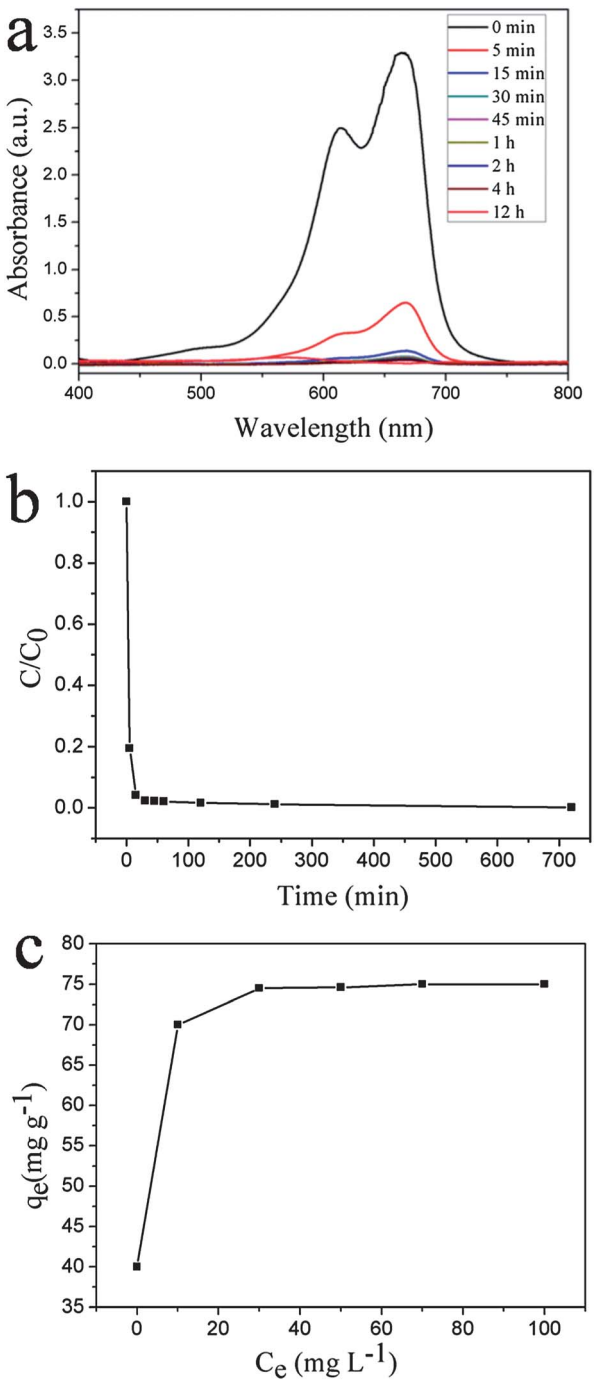

Fig. 8 (a) Absorption spectra of an aqueous solution of MB (20 mg L^{-1}, 10 mL) in the presence of as-prepared tungsten trioxide products (10 mg) at different time intervals. (b) Adsorption rate of MB on the as-prepared tungsten trioxide products. (c) Adsorption isotherm of MB on the as-prepared tungsten trioxide products.

Generally speaking, it is accepted that the WO_3 nanotubes with small pore diameters should possess a much larger BET surface area. This phenomena may be understood by taking the following considerations. Based on the above FTIR results, the nanotubes will not be blocked by SO_4^{2-} ions, and thus we believe that many nanotubes are too long to be filled completely

by liquefied nitrogen (Scheme S1†), which will lead to unsaturated nitrogen adsorption in the nanotubes, and consequently display a smaller BET surface area. On the other hand, a much bigger intrinsic relative density (7.2 g cm^{-3}) also leads to a smaller BET surface area and pore volume, as well as micropore area.

Based on the investigations described above and the experimental results, we believe that the formation mechanism of the WO_3 nanotube bundles may be rationally interpreted by curling and self-assembly processes (Scheme 1). Firstly, H_2WO_4 was formed after $NaHSO_4$ and Na_2WO_4 were added into deionized water at room temperature. It consists of layers of [WO_6] octahedra, which share their four equatorial oxygen atoms. The layers are linked to each other through hydrogen bonds, which are derived from the interaction of water molecules and oxygen atoms in the axial positions of octahedral [WO_6] with the neighboring layers. Owing to the lamellar structure separated by crystal water molecules, H_2WO_4 tends to form slice-like nanocrystals.[9] Naturally, the WO_3 slices were obtained when the reaction temperature exceeded the decomposition temperature of H_2WO_4. Furthermore, as with TiO_2,[19] the surface of WO_3 contains many hydroxyl groups. Because H^+ ions have a much stronger interaction with WO_3 than Na^+ ions through hydrogen bonding interactions, namely, the W–OH$\cdots H^+$ is more stable than W–OH$\cdots Na^+$, H^+ ions will be easily adsorbed on the surface of WO_3 slices in comparison. The well-ordered and layered tungsten trioxide slices could be self-assembled by the static electric link between SO_4^{2-} ions and H^+ ions on the slices surface. Then, the sodium ions (Na^+) are inserted into the layers; it should be noted that most of the Na^+ ions exist between the two slices, and only a few Na^+ ions are on one side of the outer WO_3 slice due to the fast diffusion of the outer Na^+. Subsequently, these slices began to gradually curl by the repel force of static electricity between the Na^+ and H^+ on the surface of the WO_3 slices, owing to a charge imbalance, and the nanotube appeared with an uninterrupted rolling of a WO_3 outer-slice. The curling process continued and produced more nanotubes. Finally, the as-produced nanotubes orderly congregated to form WO_3 nanotube bundles, through a process of self-assembly, with the help of SO_4^{2-} ions. Although the bundle structure is stable, it can be converted into free nanotubes under a long treatment time of aqueous ultrasonication (Fig. 7).

To better understand the formation mechanism, a series of experiments were carried out. Further experiments indicate that the forming of WO_3 nanotube bundles depends highly on the initial reagent $NaHSO_4$. While other conditions remain unchanged, other inorganic salts such as NH_4HSO_4 and $KHSO_4$ were used instead of $NaHSO_4$ in the reaction system. As a result, not only were WO_3 nanotube bundles not obtained, but also the crystallization changed greatly (Fig. S1 and S2†). Notably, it turns out that the Na^+ ions play a critical role in the shape-control processes, and the nucleation ability of Na^+ ions is much stronger than K^+ ions or NH_4^+ ions. Taking K^+ ions as an example, K^+ and Na^+ ions, in the form of hydrated ions in aqueous solution, may serve as the bond bridge between the growth units to form a crystal nucleus. Because the hydrated ionic radii of the Na^+ ion (0.36 nm) is larger than that of the K^+ ion (0.24 nm), every Na^+ hydrated ion can attract more precursor clusters than the K^+ hydrated ion. Therefore, at the same concentration of reagents, the Na^+ ion could remarkably influence the morphology and crystal structure of the products.[20] In addition, a certain amount of Na^+ ions are required as a stabilizing ion for the formation of h-WO_3,[21] and the Na^+ ion, with a higher charge density than the K^+ and NH_4^+ ions, can promote strongly the curling of the WO_3 nanoslice. According to previous literature,[22] sulfates significantly influence WO_3 morphology. Recently, Gu *et al.* have reported a controllable hydrothermal method for the assembly of tungsten oxide nanorods/nanowires into well-defined two- and three-dimensional nanostructures by adding different sulfates, and proposed a sulfate-induced oriented attachment growth mechanism for the possible formation mechanism.[10] The oriented attachment mechanism requires that the adjacent nanoparticles are self-assembled by sharing a common crystallographic orientation, and the fusing of these particles at a planar interface.[23] The formation mechanism of the nanotube bundles that we proposed is similar to the above mentioned, but some difference still exists. As shown in Fig. 2c and 7, broken nanotubes cannot be observed, which indicates that two individual nanotubes will not coalesce together by an oriented attachment mechanism. In our system, the SO_4^{2-} ions also play many key roles in directing the morphology of the final crystals, with two major functions, achieved by keeping the charge in balance through electrostatic interactions. One is templating the formation of the WO_3 ordered and layered structure, another is constructing the nanotube bundles from nanotubes *via* a self-assembly process but oriented attachment.

Fig. 6 also supports the formation mechanism of the WO_3 nanotube bundles described in Scheme 1. Unexpectedly, some residual layered slices (Fig. 6) can be found in the reaction system, implying that the nanotube bundle is generated from layered slices. However, it should be mentioned that not all slices can form nanotubes, only those which are ribbon-like and have rectangular superstructures can perform this curling easily.[24] Obviously, it is a regular rectangle slice that can form a nanotube. On the contrary, irregular slices in Fig. 6 cannot be converted into nanotubes.

It is interesting to observe that the bundles can be disassembled by exposure to a long aqueous ultrasonication time. As shown in Fig. 7, in some nanotube bundles and free nanotubes from bundles, the disassembly can be clearly observed. These results proved further that the obtained samples are assembled from numerous nanotubes, and these nanotubes are not tightly connected to each other by sharing the same face. It is worth mentioning that if the time of aqueous ultrasonication is relatively short, the WO_3 bundles will be partially disassembled. On the contrary, the bundles can be disassembled completely with long time aqueous ultrasonication, as presented in Fig. 2c and Fig. 7. Additionally, it is clearly seen that some nanotubes are bent slightly, which indicates that the nanotubes possess some tenacity. It is reasonable to deduce that the nanotube bundles evolve from the separate nanotubes depending on the self-assembly process. Hence, WO_3 nanotube bundles can still keep their original aggregation after template

(SO_4^{2-}) removal, this being attributed to the link of supramolecular forces (hydrogen bonds and van der Waals force) between the nanotubes. However, this stable structure can be disassembled over a long (about 30 min) treatment time of aqueous ultrasonication.

3.1 Adsorption performance in water treatment

To evaluate the potential application in water treatment of WO_3 nanotube bundles assembled by nanotubes, the adsorption capacities for the organic pollutant were investigated. Methylene blue (MB), a common cationic dye that has been widely used in the textile industry, was chosen as a model organic water pollutant. The characteristic absorption of MB at 664 nm was chosen as the indicator to be monitored during the adsorption process. Fig. 8a shows the absorption spectra of an aqueous solution of MB in the presence of WO_3 nanotube bundles at different time intervals, which shows that the MB could be removed almost completely in a short time. The relation between the adsorption capacity of the WO_3 nanotube bundles and the initial concentration of MB is shown by the adsorption isotherm in Fig. 8b. A Langmuir adsorption model was used to represent the relationship between the amount of MB adsorbed at equilibrium (q_e, mg g^{-1}) and the equilibrium solute concentration (C_e, mg L^{-1}),[25]

$$q_e = q_m b C_e/(1 + bC_e) \quad (1)$$

where q_m (mg g^{-1}) is the maximum adsorption capacity corresponding to complete monolayer coverage and b is the equilibrium constant (L mg^{-1}). When such a model was adopted to analyze the adsorption isotherm, it can be observed that the adsorption capacity of MB by the as-synthesized WO_3 nanotube bundles is about 75 mg g^{-1} (Fig. 8c), which showed a much higher adsorption performance than the commercial tungsten oxide particles (12.37 mg g^{-1}).[26] Compared to those of previously reported transition metal oxides including Mn_3O_4,[27] Fe_2O_3,[28] and MnO_2,[29] as well as other alternative adsorbents such as MCM-22,[30] fly ash,[31] and red mud,[32] the adsorption capability of our tungsten trioxide nanostructure was also much higher than them. This suggests that the as-prepared tungsten trioxide has good potential as an efficient adsorbent material for organic wastewater treatment applications. The enhanced performance could be largely attributed to the electrostatic attraction between the tungsten trioxide surface and the MB species.

4 Conclusions

In summary, using a hydrothermal strategy based on a two step self-assembly mechanism, we have successfully fabricated uniform and stable WO_3 nanotube bundles which are able to be disassembled. It is a facile route that involves no seeds, catalysts, or traditional templates and is feasible for the low-cost and large-scale production of WO_3 nanotubes. It turns out that $NaHSO_4$ has a crucial influence on the crystallization and morphology of the obtained product, which cannot be replaced by NH_4HSO_4 or $KHSO_4$. Most importantly, among Na^+, NH_4^+ and K^+ ions, only the Na^+ ion can be of benefit for the formation of the WO_3 nanosheet. Additionally, only SO_4^{2-} ions were the junction between different nanosheets or nanotubes to control the self-assembly processes. Hence, the Na^+, H^+ and SO_4^{2-} ions serve as special multifunctional agents to make a serial of self-assembly conversion: ordered layered nanosheets (3D) into nanotubes (1D) into nanotube bundles (3D). The as-prepared tungsten trioxide products show a good ability to remove an organic pollutant in wastewater, and are expected to be useful in many other applications.

Acknowledgements

This project is supported financially by the National Natural Science Foundation of China (no. 51272107), the Natural Science Foundation of Jiangsu Province, China (no. BK2011024, BK2012035) and a project funded by the Priority Academic Program Development (PAPD) of Jiangsu Higher Education Institutions.

Notes and references

1 A. Yella, M. N. Tahir, S. Meuer, R. Zentel, R. Berger, M. Panthöfer and W. Tremel, *J. Am. Chem. Soc.*, 2009, **131**, 17566; Y. G. Su, L. P. Li and G. S. Li, *Chem. Commun.*, 2008, 4004; M. Law, L. E. Greene, J. C. Johnson, R. Saykally and P. D. Yang, *Nat. Mater.*, 2005, **4**, 455; W. Cai, A. R. Hsu, Z. B. Li and X. Chen, *Nanoscale Res. Lett.*, 2007, **2**, 265.

2 H. G. Choi, Y. H. Jung and D. K. Kim, *J. Am. Ceram. Soc.*, 2005, **88**, 1684; G. Z. Shen, J. Xu, X. F. Wang, H. T. Huang and D. Chen, *Adv. Mater.*, 2011, **23**, 771; W. Lu, P. Gao, W. B. Jian, Z. L. Wang and J. Fang, *J. Am. Chem. Soc.*, 2004, **126**, 14816; R. E. Algra, M. A. Verheijen, M. T. Borgstrom, L. F. Feiner, G. Immink, W. J. P. van Enckevort, E. Vlieg and E. P. A. M. Bakkers, *Nature*, 2008, **456**, 369; D. Chen, J. Xu, Z. Xie and G. Z. Shen, *ACS Appl. Mater. Interfaces*, 2011, **3**, 2112; Y. Liu, Y. Gao, Q. H. Lu, Y. F. Zhou and D. Y. Yan, *Nanoscale*, 2012, **4**, 224.

3 Z. Tang and N. A. Kotov, *Adv. Mater.*, 2005, **17**, 951; B. Liu and H. C. Zeng, *J. Am. Chem. Soc.*, 2004, **126**, 8124.

4 Y. Y. Bao, L. H. Bi, L. X. Wu, S. S. Mal and U. Kortz, *Langmuir*, 2009, **25**, 13000; C. Z. Yuan, X. G. Zhang, L. H. Su, B. Gao and L. F. Shen, *J. Mater. Chem.*, 2009, **19**, 5772; Y. H. Ni, R. R. Puthenkovilakom and Q. Huo, *Langmuir*, 2004, **20**, 2765; S. Y. Tu, S. H. Kim, J. Joseph, D. A. Modarelli and J. R. Parquette, *J. Am. Chem. Soc.*, 2011, **133**, 19125; X. Wang, X. L. Wu, Y. G. Guo, Y. T. Zhong, X. Q. Cao, Y. Ma and J. N. Yao, *Adv. Funct. Mater.*, 2010, **20**, 1680; S. G. Jang, E. J. Kramer and C. J. Hawker, *J. Am. Chem. Soc.*, 2011, **133**, 16986; S. Pal, Z. T. Deng, H. N. Wang, S. L. Zou, Y. Liu and H. Yan, *J. Am. Chem. Soc.*, 2011, **133**, 17606.

5 R. H. Baughman, A. A. Zakhidovde and W. A. Heer, *Science*, 2002, **297**, 787; L. Hueso and N. Mathur, *Nature*, 2004, **427**, 301; S. J. Son, J. Reichel, B. He, M. Schuchman and S. B. Lee, *J. Am. Chem. Soc.*, 2005, **127**, 7316; D. Li and Y. N. Xia, *Nano Lett.*, 2004, **4**, 933.

6 S. Hu and X. Wang, *J. Am. Chem. Soc.*, 2008, **130**, 8126; L. Shi and H. L. Lin, *Langmuir*, 2011, **27**, 3977; A. W. Xu, Y. P. Fang, L. P. You and H. Q. Liu, *J. Am. Chem. Soc.*, 2003, **125**, 1494; I. S. Cho, S. Lee, J. H. Noh, D. W. Kim, H. S. Jung, D. Kim and W. Hong, *Cryst. Growth Des.*, 2010, **10**, 2447; C. O'Dwyer, D. Navas, V. Lavayen, E. Benavente, M. A. Santa Ana, G. González, S. B. Newcomb and C. M. Sotomayor Torres, *Chem. Mater.*, 2006, **18**, 3016; D. Kim, A. Ghicov, S. P. Albu and P. Schmuk, *J. Am. Chem. Soc.*, 2008, **130**, 16454; X. F. Yang, H. Tang, K. S. Cao, H. J. Song, W. C. Sheng and Q. Wu, *J. Mater. Chem.*, 2011, **21**, 6122.

7 J. Zhang, J. P. Tu, X. H. Xia, X. L. Wang and C. D. Gu, *J. Mater. Chem.*, 2011, **21**, 5492; Z. H. Jiao, X. W. Sun, J. M. Wang, L. Ke and H. V. Demir, *J. Phys. D: Appl. Phys.*, 2010, **43**, 285501; M. Sadakane, K. Sasaki, H. Kunioku, B. Ohtani, W. Ueda and R. Abe, *Chem. Commun.*, 2008, 6552; Z. Xie, Y. G. Zhu, J. Xu, H. T. Huang, D. Chen and G. Z. Shen, *CrystEngComm*, 2011, **13**, 6393; R. S. Vemuri, K. K. Bharathi, S. K. Gullapalli and C. V. Ramana, *ACS Appl. Mater. Interfaces*, 2010, **2**, 2623; Q. Xiang, G. F. Meng, H. B. Zhao, Y. Zhang, H. Li, W. J. Ma and J. Q. Xu, *J. Phys. Chem. C*, 2010, **114**, 2049; V. Cristino, S. Caramori, R. Argazzi, L. Meda, G. L. Marra and C. A. Bignozzi, *Langmuir*, 2011, **27**, 7276.

8 M. Breedon, P. Spizzirri, M. Taylor, J. Plessis, D. McCulloch, J. M. Zhu, L. S. Yu, Z. Hu, C. Rix, W. Wlodarski and K. Kalantar-zadeh, *Cryst. Growth Des.*, 2010, **10**, 430; E. K. Heidari, E. Marzbanrad, C. Zamani and B. Raissi, *Nanoscale Res. Lett.*, 2010, **5**, 370; F. B. Hiller, R. Lungwitz, A. Seifert, M. Hietschold, M. Schlesinger, M. Mehring and S. Spange, *Angew. Chem., Int. Ed.*, 2009, **48**, 8878; S. H. Baeck, K. S. Choi, T. F. Jaramillo, G. D. Stucky and E. W. McFarland, *Adv. Mater.*, 2003, **15**, 1269; H. S. Pokhrel, J. Birkenstock, M. Schowalter, A. Rosenauer and L. Meadler, *Cryst. Growth Des.*, 2010, **10**, 632; Z. G. Zhao and M. Miyauchi, *J. Phys. Chem. C*, 2009, **113**, 6539; B. Yang, Y. J. Zhang, E. Drabarek, P. Barnes and V. Luca, *Chem. Mater.*, 2007, **19**, 5664; R. W. Morales, M. Cason, O. Aina, N. Tacconi and K. Rajeshwar, *J. Am. Chem. Soc.*, 2008, **130**, 6318; C. Santato, M. Odziemkowski, M. Ulmann and J. Augustynski, *J. Am. Chem. Soc.*, 2001, **123**, 10639.

9 J. Zhu, S. L. Wang, S. H. Xie and H. X. Li, *Chem. Commun.*, 2011, **47**, 4403; J. M. Ma, J. Zhang, S. R. Wang, T. H. Wang, J. B. Lian, X. C. Duan and W. J. Zheng, *J. Phys. Chem. C*, 2011, **115**, 18157; G. Wang, Y. Ji, X. R. Huang, X. Q. Yang, P. I. Gouma and M. Dudley, *J. Phys. Chem. B*, 2006, **110**, 23777; N. D. Hoa and S. A. EI-Safty, *Nanotechnology*, 2011, **22**, 485503; Z. G. Zhao and M. Miyauchi, *Angew. Chem., Int. Ed.*, 2008, **47**, 7051; J. M. Wang, E. Khoo, P. S. Lee and J. Ma, *J. Phys. Chem. C*, 2009, **113**, 9655; M. Shibuya and M. Miyauchi, *Adv. Mater.*, 2009, **21**, 1373.

10 J. Polleux, A. Gurlo, N. Barsan, U. Weimar, M. Antonietti and M. Niederberger, *Angew. Chem., Int. Ed.*, 2005, **45**, 261; J. Polleux, N. Pinna, M. Antonietti and M. Niederberger, *J. Am. Chem. Soc.*, 2005, **127**, 15595; Z. J. Gu, T. Y. Zhai, B. F. Gao, X. H. Sheng, Y. B. Wang, H. B. Fu, Y. Ma and J. N. Yao, *J. Phys. Chem. B*, 2006, **110**, 23829; J. M. Wang, E. Khoo, P. S. Lee and J. Ma, *J. Phys. Chem. C*, 2008, **112**, 14306.

11 M. T. Chang, L. J. Chou, Y. L. Chueh, Y. C. Lee, C. H. Hsieh, C. D. Chen, Y. W. Lan and L. J. Chen, *Small*, 2007, **3**, 658.

12 J. H. Ha, P. Muralidharan and D. K. Kim, *J. Alloys Compd.*, 2009, **475**, 446.

13 M. F. Daniel, B. Desbat, J. C. Lassegues, B. Gerand and M. Figlarz, *J. Solid State Chem.*, 1987, **67**, 235.

14 G. L. Frey, A. Rothschild, J. Sloan, R. Rosentsveig, R. Popovitz-Biro and R. Tenne, *J. Solid State Chem.*, 2001, **162**, 300.

15 J. H. Choy, Y. Kim, B. W. Kim, N. G. Park, G. Campet and J. C. Grenier, *Chem. Mater.*, 2000, **12**, 2950.

16 L. Liu, J. Jiang, S. M. Jin, Z. M. Xia and M. T. Tang, *CrystEngComm*, 2011, **13**, 2529; A. Rajbanshi, B. A. Moyer and R. Custelcean, *Cryst. Growth Des.*, 2011, **11**, 2702.

17 S. M. Kanan, Z. X. Lu, J. K. Cox, G. Bernhardt and C. P. Tripp, *Langmuir*, 2002, **18**, 1707.

18 X. Chen, Y. F. Shen, S. L. Suib and C. L. O' Young, *Chem. Mater.*, 2002, **14**, 940; P. Z. Araujo, V. Luca, P. B. Bozzano, H. L. Bianchi, G. Soler-Illia and M. A. Blesa, *ACS Appl. Mater. Interfaces*, 2010, **2**, 1663.

19 H. Lin, J. Long, Q. Gu, W. Zhang, R. Ruan, Z. Li and X. Wang, *Phys. Chem. Chem. Phys.*, 2012, **14**, 9468; A. Ramakrishnan, S. Neubert, B. Mei, J. Strunk, L. Wang, M. Bledowski, M. Muhler and R. Beranek, *Chem. Commun.*, 2012, **48**, 8556; F. Yang, J. Y. Yao, F. L. Liu, H. C. He, M. Zhou, P. Xiao and Y. H. Zhang, *J. Mater. Chem. A*, 2012, DOI: 10.1039/c2ta00055e.

20 L. Zheng, Y. Xu, D. Jin and Y. Xie, *Chem. Mater.*, 2009, **21**, 5681.

21 X. Wang and Y. D. Li, *J. Am. Chem. Soc.*, 2002, **124**, 2880; G. R. Patzke, A. Michailovski, F. Krumeich, R. Nesper, J. D. Grunwaldt and A. Baiker, *Chem. Mater.*, 2004, **16**, 1126; K. Huang, Q. T. Pan, F. Yang, S. B. Ni, X. C. Wei and D. He, *J. Phys. D: Appl. Phys.*, 2008, **41**, 155417.

22 S. Rajagopal, D. Nataraj, D. Mangalaraj, Y. Djaoued, J. Robichaud and O. Yu, *Nanoscale Res. Lett.*, 2009, **4**, 1335; X. C. Song, Y. F. Zheng, E. Yang and Y. Wang, *Mater. Lett.*, 2007, **61**, 3904; Z. J. Gu, Y. Ma, W. S. Yang, G. J. Zhang and J. N. Yao, *Chem. Commun.*, 2005, 3597.

23 Q. Zhang, S. J. Liu and S. H. Yu, *J. Mater. Chem.*, 2009, **19**, 191; R. L. Penn and J. F. Banfield, *Science*, 1998, **281**, 969; J. Zhang, F. Huang and Z. Lin, *Nanoscale*, 2010, **2**, 18.

24 X. Peng, L. Manna, W. Yang, J. Wickham, E. Scher, A. Kadavanich and A. P. Alivisatos, *Nature*, 2000, **404**, 59; M. Li, H. Schnablegger and S. Mann, *Nature*, 1999, **402**, 393.

25 R. C. Wu, J. H. Qu and Y. S. Chen, *Water Res.*, 2005, **39**, 630.

26 S. Jeon and K. Yong, *J. Mater. Chem.*, 2010, **20**, 10146.

27 H. Chen and J. He, *J. Phys. Chem. C*, 2008, **112**, 17540.

28 L. Zhong, J. Hu, H. Liang, A. Cao, W. Song and L. Wan, *Adv. Mater.*, 2006, **18**, 2426.

29 J. Fei, Y. Cui, X. Yan, W. Qi, Y. Yang, K. Wang, Q. He and J. Li, *Adv. Mater.*, 2008, **20**, 452.

30 S. Wang, H. Li and L. Xu, *J. Colloid Interface Sci.*, 2006, **295**, 71.

31 V. K. Gupta, D. Mohan, S. Sharma and M. Sharma, *Sep. Sci. Technol.*, 2000, **35**, 2097.

32 S. Wang, Y. Boyjoo, A. Choueib and Z. H. Zhu, *Water Res.*, 2005, **39**, 129.